BMC Infectious Diseases

RESEARCH Open Access

Infection route influence the consequences of *Nocardia farcinica* infection in BALB/c mice

Jirao Shen[1], Lichao Han[2], Jiang Yao[3], Xiaotong Qiu[1], Shuai Xu[1], Xueping Liu[1], Fang Li[4] and Zhenjun Li[1*]

Abstract

Background *Nocardia*, a rare but potentially fatal pathogen, can induce systemic infections with diverse manifestations. This study aimed to investigate the tissue and organ damage caused by *Nocardia farcinica* (*N. farcinica*) in mice via different infection routes, evaluate the resulting host immune responses, and assess its invasiveness in brain tissue.

Methods BALB/c mice were infected with *N. farcinica* through intranasal, intraperitoneal, and intravenous routes (doses: 1 × 10^8, 1 × 10^7, 1 × 10^7 CFU in 50 µl PBS). Over a 7-day period, body temperature, weight, and mortality were monitored, and samples were collected for histopathological analysis and bacterial load assessment. Serum was isolated for cytokine detection via ELISA. For RNA-seq analysis, mice were infected with 1×10^7 CFU through three infection routes, after which brain tissue was harvested.

Results Intraperitoneal and intravenous *N. farcinica* infections caused significant clinical symptoms, mortality, and neural disruption in mice, resulting in severe systemic infection. Conversely, intranasal infection primarily affected the lungs without causing significant damage to other organs. Intraperitoneal and intravenous infections significantly increased serum cytokines, particularly TNF-α and IFN-γ. RNA-seq analysis of brains from intravenously infected mice revealed significant differential gene expression, whereas the intranasal and intraperitoneal routes showed limited differences (only three genes). The enriched Kyoto Encyclopedia of Genes and Genomes (KEGG) pathways in the intravenous group were primarily related to immune processes.

Conclusion The study demonstrated that intravenous *N. farcinica* infection induces significant clinical symptoms, triggers an inflammatory response, damages multiple organs, and leads to systemic infections.

Keywords Different infection routes, *Nocardia farcinica*, Pathological change, Transcriptomic analysis

*Correspondence:
Zhenjun Li
lizhenjun@icdc.cn
[1]State Key Laboratory of Infectious Disease Prevention and Control, National Institute for Communicable Disease Control and Prevention, Chinese Center for Disease Control and Prevention, Beijing, China
[2]Department of Pulmonary and Critical Care Medicine, Shandong Provincial Hospital Affiliated to Shandong First Medical University, Jinan, China
[3]School of Laboratory Medicine and Life Sciences, Wenzhou Medical University, Wenzhou, China
[4]Department of Medicine, Tibet University, Lhasa, Tibet 850000, PR China

© The Author(s) 2024. **Open Access** This article is licensed under a Creative Commons Attribution-NonCommercial-NoDerivatives 4.0 International License, which permits any non-commercial use, sharing, distribution and reproduction in any medium or format, as long as you give appropriate credit to the original author(s) and the source, provide a link to the Creative Commons licence, and indicate if you modified the licensed material. You do not have permission under this licence to share adapted material derived from this article or parts of it. The images or other third party material in this article are included in the article's Creative Commons licence, unless indicated otherwise in a credit line to the material. If material is not included in the article's Creative Commons licence and your intended use is not permitted by statutory regulation or exceeds the permitted use, you will need to obtain permission directly from the copyright holder. To view a copy of this licence, visit http://creativecommons.org/licenses/by-nc-nd/4.0/.

Introduction

Nocardia, a Gram-positive pathogenic bacterium, is widely distributed in the environment, including soil, dust, water, and organic materials of animal origin [1]. *Nocardia farcinica (N. farcinica)* is widely distributed in the United States and also is the most common *Nocardia* species in China. It is considered one of the most common causative agents among *Nocardia* spp [2]. *N. farcinica* can invade the lungs destructively, leading to pulmonary abscesses, necrotizing pneumonia, and other pulmonary diseases [3]. It can disseminate through the bloodstream upon entering the host organism, affecting various organs, including the joints, eyes, heart, kidneys, and central nervous system (CNS) [4]. Therefore, *N. farcinica* is considered the most pathogenic species within the *Nocardia* genus due to its high morbidity, invasiveness, and variable resistance to antimicrobial agents [5].

The main route of *Nocardia* infection is through the respiratory tract [6], and it also has a propensity to disseminate hematogenously [7]. A systematic review of *Nocardia* bacteremia found that 29% of patients had intravascular device [8]. Additionally, intraperitoneal infection is another pathway for various bacteria to invade the body [9]. *Nocardia* can enter peritoneal cavity via a peritoneal dialysis catheter instead of the bloodstream, leading to peritonitis [10]. Gastrointestinal colonization has rarely been reported, typically the due to the inhalation of spores or swallowing of sputum [11]. There is no conclusive evidence of person-to-person transmission of *Nocardia* infections [11]. The extent of host damage caused by pathogens varies depending on the infection route [12]. For example, in adult mouse models of leptospirosis, factors such as serotype, inoculation dose, and route of infection significantly influence the disease progression kinetics [13]. In addition, Michelle Nelson et al. indicates that the therapeutic effectiveness of Co-Trimoxazole in treating melioidosis depends on the infection route [14]. Therefore, understanding how different infection routes of *Nocardia* affect organisms, as studied through mouse models, is crucial for comprehending and preventing Nocardiosis. Despite its relatively low prevalence, *Nocardia* should not be overlooked due to its potential to be fatal in immunosuppressed patients [15]. A thorough understanding of *Nocardia* infection mechanisms is essential for developing guidelines to control the diseases it can cause.

Reports have confirmed the susceptibility of *Nocardia* to the CNS [16]. *Nocardia* can be isolated in the early stages after brain tissue invasion but becomes undetectable beyond 12 days post-infection (dpi). However, symptoms resembling motor dysfunction, similar to those in Parkinson's disease, persist and can last throughout the lifespan of most mice [17]. It remains unconfirmed whether all infection routes induce CNS symptoms. Furthermore, the pathogenic mechanisms of *Nocardia* in the brain have not been systematically elucidated in previous studies.

Materials and methods

Animal

Pathogen-free female BALB/c mice (6–8 weeks of age) were purchased from SPF Biotechnology Co., Ltd. (Beijing, China). Before the experiments, the mice were provided food and water ad libitum for 5 to 7 days in a sterile environment to acclimate to the microisolator cages.

Bacteria and infection of mice

N. farcinica IFM 10,152 was sourced from the German Resource Centre for Biological Materials (Brunswick, Germany). *N. farcinica* was cultured to the exponential phase in BHI broth (Oxoid Ltd, Hants, UK) at 37 °C before infection experiments. At the time of the experiment, the mice were 7–9 weeks old and had body weights of 18.9±0.9 g (mean±SD). The mice were divided into three groups: intranasal infection, intraperitoneal injection, and intravenous injection, with 40 mice in each group. Each group was further subdivided into a PBS control group and 1, 3, and 7 dpi groups, with 10 mice in each subgroup. The intranasal, intraperitoneal, and tail vein groups received a uniform bacterial suspension containing approximately1×10^8, 1×10^7, and 1×10^7 colony-forming units (CFU) in 50 µl via intranasal administration, intraperitoneal injection, and intravenous injection, respectively. Control groups received an equal volume of sterile PBS via the same routes. The 7-day post-infection groups were also assessed for mortality, body temperature, and weight changes. During the intranasal infection procedure, mice were anesthetized with sodium pentobarbital at a dose of 1 to 1.2 mg per mouse. At the designated time point, mice were euthanized via cervical dislocation, and relevant tissues and serum samples were collected.

For transcriptomics research, mice were infected with 1×10^7 CFU through three routes. Brain tissues were collected at 7 dpi. Based on clinical symptom observations, it can be deduced that the control groups for all three infection routes had no significant impact on the mice. Consequently, histopathological examination and transcriptomic study employed intraperitoneal infection of the same volume of PBS as the control group.

Body temperature and weight

Body temperature and weight were serially quantified every day for 7 dpi with *N. farcinica* IFM 10,152, and the

initial values were also measured. Mice were weighed to the nearest thousandth of a gram, and body temperature was measured using an Animal Thermometer (KEW, Nanjing, China) with rectal readings accurate to 0.1 °C.

Bacteria burden detection in tissues

For each infection route, 10 mice were sacrificed at 1, 3, and 7 dpi. The heart, liver, spleen, lung, kidney, eye, brain, and rectum tissue were collected and homogenized in 1 ml of PBS. To quantify the *N. farcinica* bacterial load in tissues, serial dilutions of the homogenized samples were plated on Brain Heart Infusion (BHI) agar and incubated at 37 °C for 48 h.

Histopathology

The tissues were fixed in 4% paraformaldehyde and embedded in paraffin. The samples were sectioned at 5 μm, stained with hematoxylin and eosin, and imaged using a biomicroscope (Nikon, Eclipse Ci-L, Japan) according to the manufacturer's instructions. Pathological analysis was conducted on the images.

ELISA detection

For serum cytokine detection, blood was obtained at 1, 3, and 7 dpi. Serum was collected after centrifugation and stored at −80 °C until testing. Cytokine concentrations (IL-4, IL-6, IL-10, TNF-α, IFN-γ) were measured by quantitative ELISA (BD OptEIA™, San Diego, CA, USA) according to the manufacturer's instructions.

Extraction of total RNA from infected animals

Total brain RNA was isolated at 7 dpi from *N. farcinica*-infected mice and PBS controls (three replicates per group) using TRIzol reagent (Invitrogen, USA). RNA concentration, RIN, and size were assessed using an Agilent 2100 Bioanalyzer (Agilent, Palo Alto, CA, USA), and purity was measured with a NanoPhotometer (Thermo Fisher, Waltham, MA, USA).

Library construction and RNA sequencing

After confirming RNA quality, magnetic beads with Oligo(dT) were used for mRNA enrichment and purification. mRNA was reverse transcribed into cDNA using random primers. The resulting cDNA fragments were then end-repaired, A-tailed, and ligated to sequencing adapters. Target fragments were purified with magnetic beads and then amplified by PCR, completing the library preparation. Preliminary quantification of the library was performed using Qubit 3.0. The sequencing strategy used was PE150.

Read mapping and analysis

Raw sequencing data (Raw Reads) from the Illumina platform were processed to obtain high-quality sequences (Clean Reads) by removing low-quality reads, adapter contamination, and reads with an N ratio greater than 5%. All subsequent analyses were performed based on the Clean Reads. All subsequent analyses were based on the Clean Reads. HISAT2, HTSeq, RSEM, and DESeq2 were used for reference genome alignment, gene expression quantification, and differential gene expression analysis, respectively.

qRT–PCR

Total RNA from repeated infection brain samples was used for qRT-PCR. qRT-PCR was performed with SYBR Premix Ex Taq II reagents (TaKaRa, Japan) on a QuantGene 9600 real-time PCR analyzer (Hangzhou Bori Technology Co., Ltd, Hangzhou, China). The housekeeping gene β-actin was used to normalize gene expression levels. Fold changes in gene expression were calculated using the $2(-\Delta\Delta Ct)$ method.

Statistical analysis and data visualization

Matlab software (MathWorks, Natick, MA) was used for data analysis and visualization. Statistical results were presented as mean±standard deviation. Analysis of variance was performed on serum cytokines in Fig. 3. Student's t-test was conducted between each experimental group and the control group, assuming homogeneity of variance and normal distribution. Differential transcriptome and functional enrichment analyses were performed using the Annocloud platform (https://c.solargenomics.com/), and Gene Ontology (GO) and KEGG charts were generated. The protein-protein interaction network was visualized using STRING (https://string-db.org) and Cytoscape software.

Result

Mice infected with *N. Farcinica* via intravenous route exhibit more severe clinical symptoms

Given that the intraperitoneal route is commonly used in lethal dose studies of pathogens, this research employed a concentration of 1×10^8 to infect mice as a positive control. Partial mortality was observed in mice at this concentration. Figure 1A shows the mortality assessment over a 7-day period. Mice in the intraperitoneal infection group exhibited messy, dull fur and reduced food and water intake after infection. At 2 dpi, the anus was blocked by excrement, resulting in suppuration and difficulty in defecation (Supplementary Fig. 1a). On the third day, increased ocular secretion made it difficult for the mice to open their eyes (Supplementary Fig. 1b). Some mice exhibited neurological symptoms during the experiment, such as head tilting and circling when their tails were lifted. Weight decreased from 1 to 5 dpi and then stabilized, while in the control group, it increased from 1 to 4 dpi and then fluctuated slightly. Body temperature

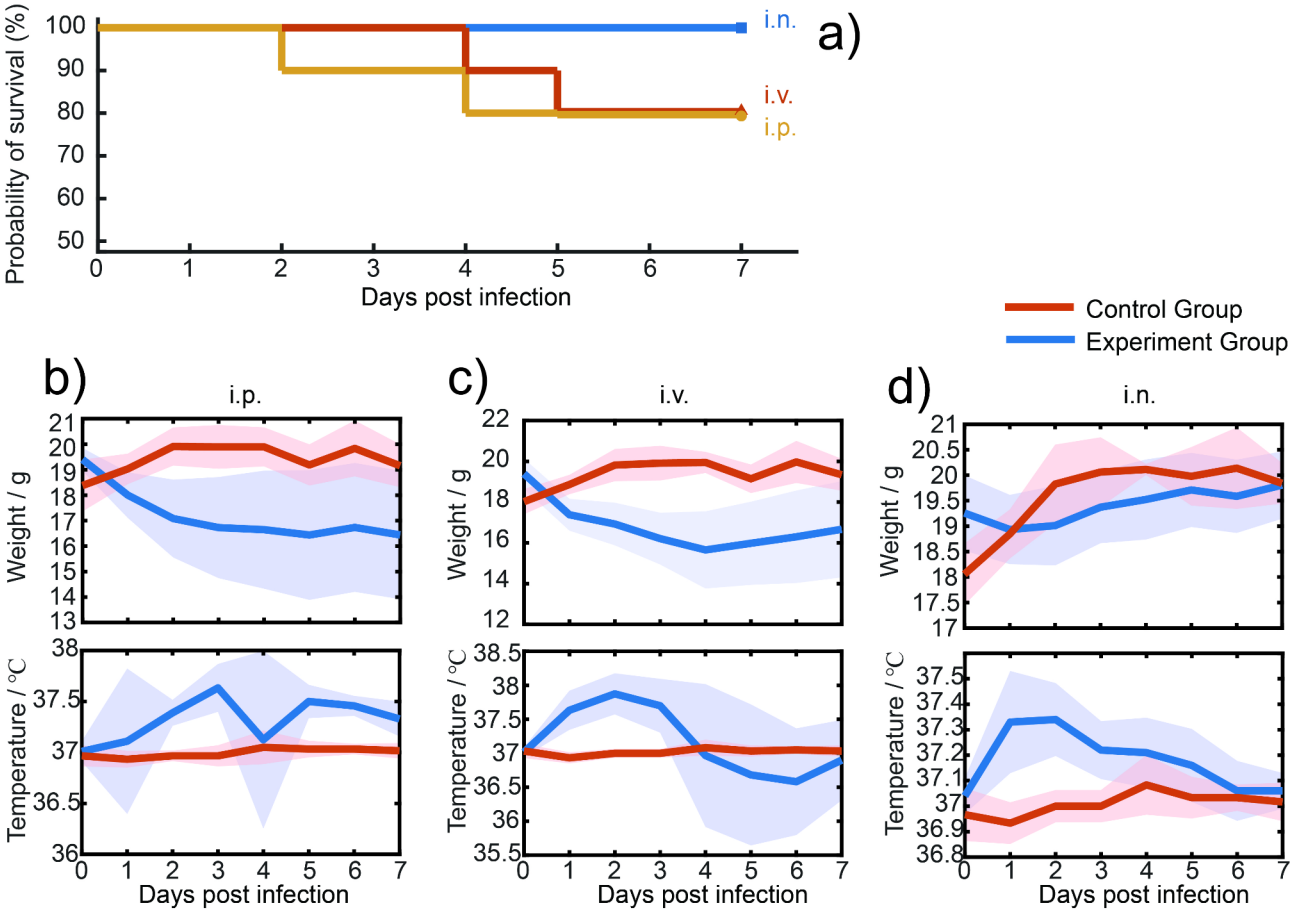

Fig. 1 Clinical symptoms analysis of BALB/c mice infected with *N. farcinica* via different routes. Female mice ($n = 10$) were infected intraperitoneally (i.p.), delivered intravenously (i.v.), and dropped intranasally (i.n.) with *N. farcinica* IFM 10,152, respectively. (**A**) Assessment of mortality in 7 consecutive days. (**B**) Body temperature and weight of i.p. group. (**C**) Body temperature and weight of i.v. group. (**D**) Body temperature and weight of i.n. group. Mice were weighed to the accuracy of thousandth of a gram. Body temperature was assessed rectal temperature to the nearest 0.1 ℃

increased from 1 to 3 dpi, followed by a gradual return to normal. Two mice experienced a sudden drop in body temperature at 1 and 4 dpi, respectively, and died at the next day. In contrast, the control group remained stable throughout (Fig. 1B).

Similar to the intraperitoneal infection group, mice in the intravenous infection group also displayed ocular and neurological symptoms. Notably, some mice in the intravenous infection group experienced a sharp drop in body temperature accompanied by neurological symptoms and died the next day. Some mice experienced a decline in body temperature, which later recovered, but neurological symptoms persisted throughout the experiment. Body temperature and weight changes in other mice are shown in Fig. 1C.

Mice in the intranasal infection group did not exhibit significant clinical symptoms during infection. Body temperature rose at 2 dpi and then decreased to normal level. Weight dropped at 2 dpi, then rose and approached that of the control group. The control group for intranasal infection was similar to the other two control groups (Fig. 1D).

Mice infected with *N. Farcinica* via intravenous route exhibit a more severe bacterial burden in tissues

As shown in Fig. 2, intranasal infection caused a high bacterial burden only in the lungs. Bacterial burdens in the spleen, lung, and rectum were higher in intraperitoneal infection compared to intravenous infection, while other tissues had lower burdens. Intravenous infection resulted in a higher bacterial load in the brain compared to the other two infection routes. In summary, bacterial burdens in all tissues of mice infected via different routes peaked at 1 dpi. An exception was the kidneys in the intravenous infection group, where the bacterial burden continued to rise from 1 to 7 dpi.

Mice infected with *Nocardia* through intravenous infection exhibited more severe inflammatory responses

As seen in Fig. 3, IL-4 and IL-6 concentrations were significantly higher in all three infection routes compared

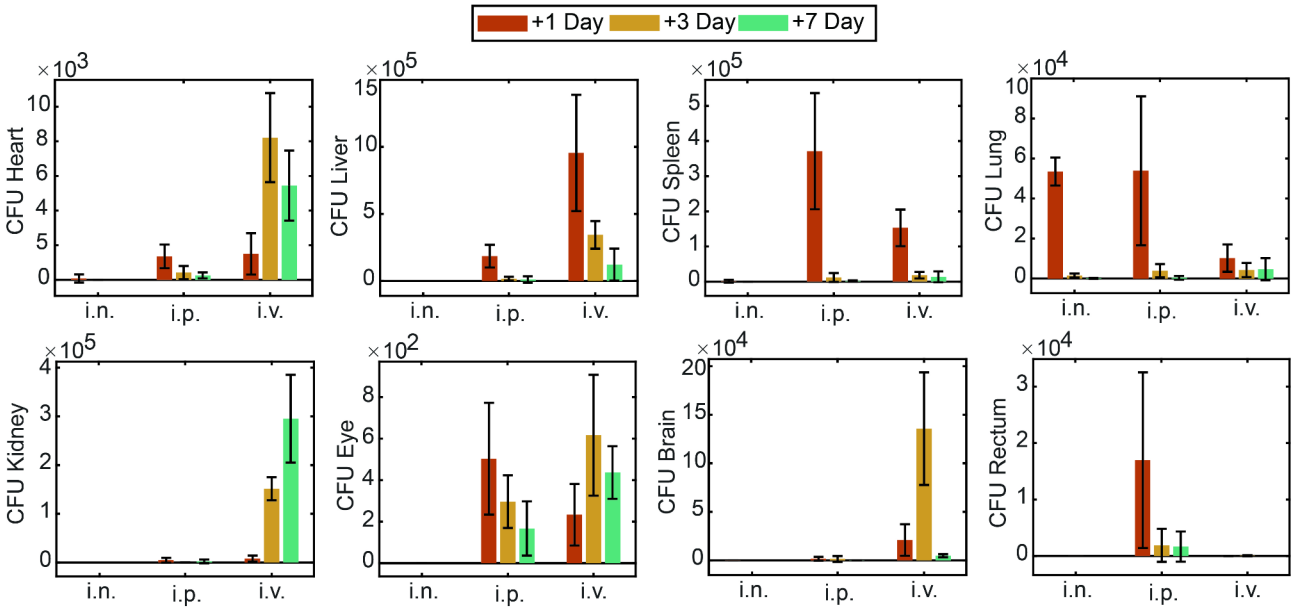

Fig. 2 The bacterial load in organs of mice infected with *N. farcinica* IFM 10,152 in different routes at 1, 3, and 7 dpi. Heart, liver, spleen, lung, kidney, eye, brain, and 5 mm long rectal were collected, and bacterial colonies in those organs were counted at 1, 3, and 7 dpi

to the control group. IL-10 expression was upregulated in the intraperitoneal and intravenous infection groups but downregulated in the intranasal group. TNF-α levels significantly increased in the intraperitoneal infection group and dramatically increased in the intravenous infection group at 3 dpi. No significant difference in expression was observed in the intranasal group. IFN-γ was significantly upregulated in the intraperitoneal infection group at 1 and 3 dpi and significantly increased at 1 dpi via intravenous infection. In the intranasal group, IFN-γ expression levels showed only minor changes.

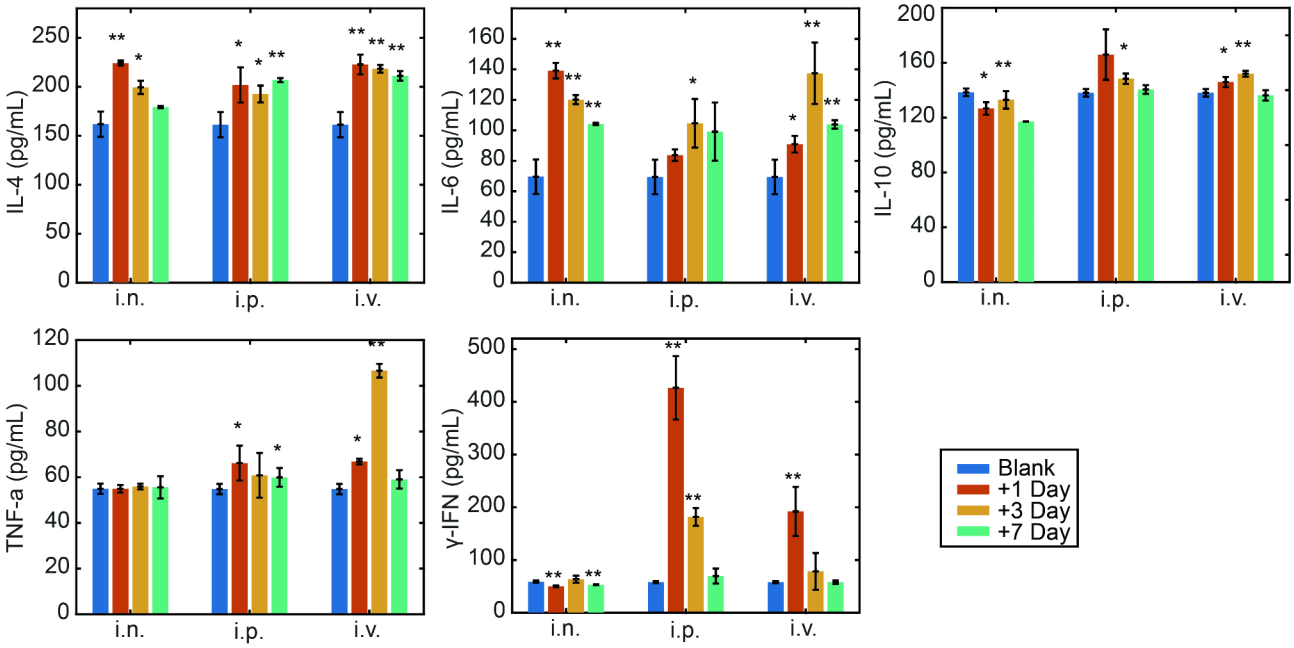

Fig. 3 The expression of serum cytokines of mice infected with *N. farcinica* IFM 10,152 in different routes at 1, 3, and 7 dpi. Mice were infected for one time with bacteria intraperitoneally (i.p.), intravenously (i.v.), and intranasally (i.n.) at a dose of 1×10^8, 1×10^7, and 1×10^7 CFU in 50 µl PBS, respectively. The data of blank group was acquired from the mice infected with 50 µl PBS at 1 dpi. Cytokine levels (IL-4, IL-6, IL-10, TNF-α, and IFN-γ) in serum were measured by ELISA. Student's t test was conducted between each experimental group and the blank group (*$P < 0.05$, **$P < 0.01$)

Histopathological analysis

Histopathological analysis revealed no obvious abnormalities or inflammation in the control group tissues. The tissue pathological changes of the main invaded organs in mice caused by *N. farcinica* with specific pathological changes are detailed in Fig. 4.

Lung

The lungs showed mild lymphocyte infiltration in multiple alveolar walls at 1 and 3 dpi (Fig. 4A, black arrow), with mild hemorrhage around local blood vessels at 7 dpi in the intraperitoneal infection group (Fig. 4A, yellow arrow). In the intravenous group, large areas of alveolar wall thickening were observed, accompanied by granulocyte infiltration (Fig. 4A, black arrow) and local hemorrhage (Fig. 4B, red arrow). No pathological changes were observed in the lungs at 1 dpi following intranasal infection; however, lymphocyte infiltration and alveolar expansion were noted at 3 and 7 dpi (Fig. 4C, yellow arrow).

Eye

The anterior corneal epithelium became thinner, with some epithelial cell nuclei shrinking and deep staining observed at 1 dpi following intraperitoneal infection. The number of corneal stromal fibroblasts increased at 1 dpi (Fig. 4A, black arrow), with punctate infiltration of lymphocytes and neutrophils appearing on the third day (Fig. 4A, yellow arrow), all of which returned to normal by day 7. At 1 day and 3 days after intravenous infection, eosinophilic reticular structures (Fig. 4B, green arrows) were observed on the cornea, with cytoplasmic loosening and slight staining (Fig. 4B, black arrow), which later returned to normal without further abnormalities. No pathological changes were observed in ocular tissue following intranasal infection.

Brain

A large number of neurons in the brain tissue shrank, with deeper staining and unclear nucleus and cytoplasm at 1 dpi following intraperitoneal infection (Fig. 4A, black arrow). Local punctate infiltration of lymphocytes and neutrophils was observed on day 3 (Fig. 4A, yellow arrow), with a small amount of neuronal degeneration on day 7. Following intravenous infection, brain tissue showed only a small amount of granulocyte infiltration at 1 dpi (Fig. 4B, black arrow) and bleeding at 3 dpi (Fig. 4B, green arrow). By day 7, focal necrosis of cortical neurons and fragmentation and dissolution of nuclei were observed (Fig. 4B, black arrow). From day 1 after intranasal infection, neurons in the brain cortex and CA3 and DG areas of the hippocampus shrank, with deeper cell staining and unclear nuclear-cytoplasmic boundaries (Fig. 4C, black arrow). This condition persisted until day 7.

Rectum

No obvious abnormalities were detected in the rectum at 1 and 3 dpi following intraperitoneal infection. Increased necrosis and dissolution of intestinal glands were observed in the local lamina propria at 7 dpi (Fig. 4A, yellow arrow). A small amount of connective tissue hyperplasia was accompanied by mild lymphocyte infiltration (Fig. 4A, red arrow). At 3 dpi following intravenous infection, intestinal tissue exhibited significant glandular dilation (Fig. 4B, red arrows) with granulocytes present within the glands (Fig. 4B, green arrows). Mild connective tissue hyperplasia in the mucosal layer, accompanied by a small amount of lymphocyte infiltration (Fig. 4B, black arrows), persisted until day 7. No pathological changes were observed in the rectum in the intranasal group.

These results suggest that intraperitoneal and intravenous infections can cause severe systemic infections in multiple organs. Histopathological analysis was also conducted on other tissues, including the heart, liver, spleen, and kidneys. Detailed results are provided in the supplementary file.

Differential gene expression statistical analysis

The selection of differentially expressed genes was primarily based on fold change values and q-values (padj values, adjusted P-values) as relevant indicators. Typically, differentially expressed genes with $|\log2 \text{ fold change}| \geq 1$ and $q < 0.05$ were considered statistically significant. Brain transcriptome data from different infection routes were compared with the control group to identify differentially expressed genes. The total number of differentially expressed genes in each comparison group is shown in Table 1.

GO functional analysis of differentially expressed genes

GO enrichment analysis revealed that of the 30 enriched terms following intravenous infection, the primary activations were related to immune processes, including pathways like G-protein coupled receptor signaling and inflammatory response. This indicates strong immune activation at the cellular membrane level, as shown by the abundance of plasma membrane components (Fig. 5A). In contrast, GO analysis of intraperitoneal injection and intranasal infection showed only 26 enriched terms with a gene count greater than 2 for each, with no overlap with GO enrichment terms from intravenous infection. This suggests that without similar widespread gene expression changes following intraperitoneal and intranasal infections, the statistical power of the enrichment analysis

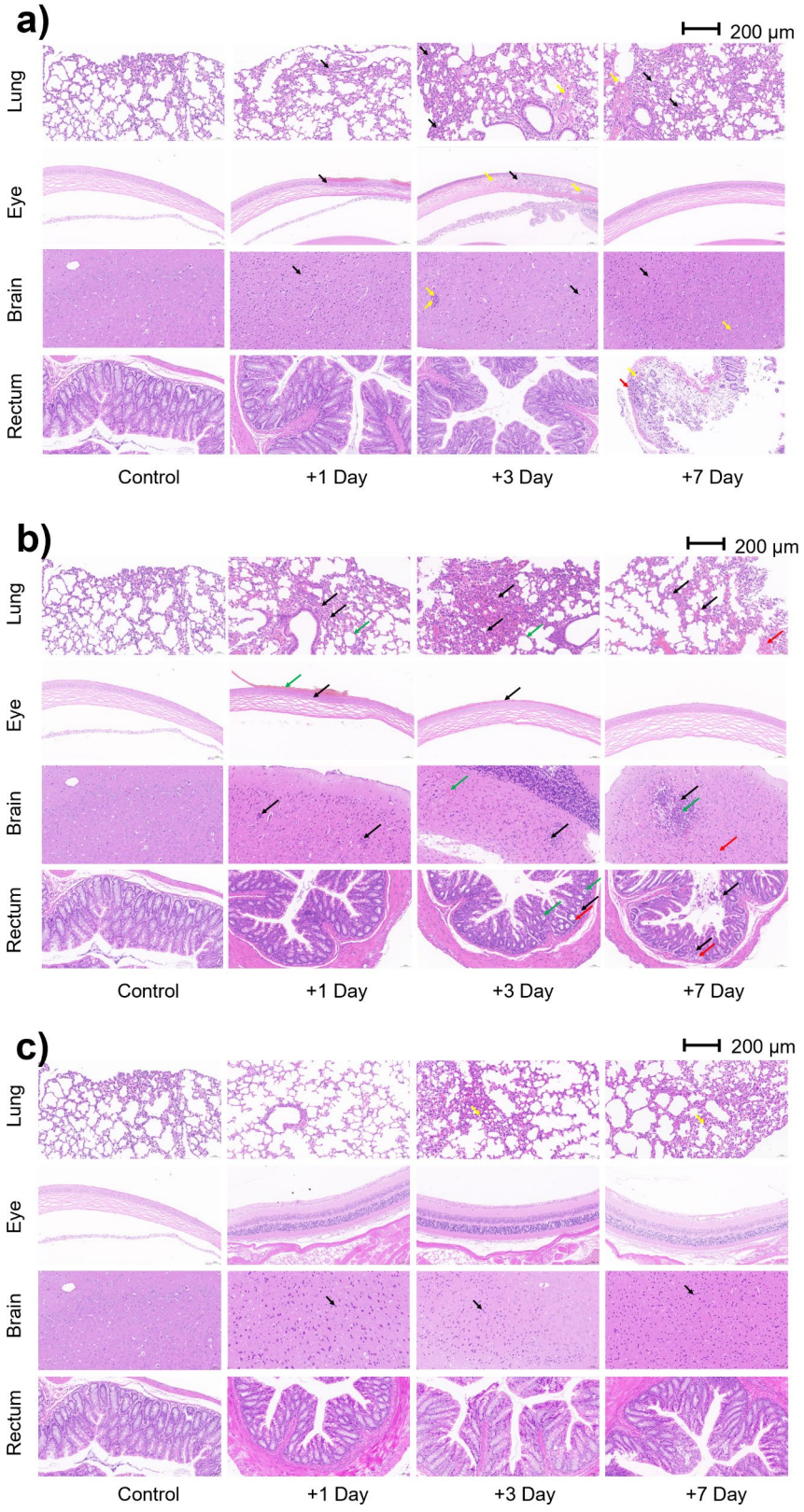

Fig. 4 Representative H&E-stained organs of mice. Scale bars: 200 μm. The arrows mark the pathological changes that were detailed described in the Results. (**A**) Mice were infected with bacteria intraperitoneally at a dose of 1×10^8 CFU in 50 μl PBS, or 50 μl PBS for 1 day. (**B**) Mice were infected with bacteria intravenous at a dose of 1×10^7, CFU in 50 μl PBS, or 50 μl PBS for 1 day. (**C**) Mice were infected with bacteria intranasally at a dose of 1×10^7, CFU in 50 μl PBS, or 50 μl PBS for 1 day

Table 1 Differentially expressed genes in each infection route

Name	i.*n.* C	i.*p.* C	i.v. C
Up	0	0	179
Down	0	3	8
Total	0	3	187

is significantly reduced, resulting in enrichment with weaker biological and statistical significance, which were therefore excluded from the GO analysis.

Differential gene expression KEGG pathway analysis

KEGG pathway enrichment analysis of brain tissue following *N. farcinica* infection reveals significant activation of immune-related pathways (Fig. 5B). Notably, the "Cytokine-cytokine receptor interaction" and "Phagosome" pathways are highly enriched, indicating a robust immune response. Additional pathways, such as "Human cytomegalovirus infection," "Epstein-Barr virus infection," and "Tuberculosis," suggest overlap with pathways involved in viral and bacterial infections. Moreover, immune signaling pathways, including "NOD-like receptor signaling" and "TNF signaling," are significantly enriched, underscoring their role in the brain's response to infection. No KEGG pathway enrichment was observed following intranasal infection, and only two pathways were enriched following intraperitoneal injection infection.

Verification of DEGs by qRT-PCR

Selected key genes from the "phagosome" and "NOD2" signaling pathways were assigned primers and subjected to qRT–PCR verification, assessing the concordance of their up- or downregulation trends with RNA-seq results. The qRT–PCR results aligned with the RNA-seq analysis, affirming the robustness of the RNA-seq data (Supplementary Fig. 4A, 4B).

Analysis of DEGs associated with nervous system disease

Transcriptomic analysis revealed that intravenous infection led to differential gene expression patterns associated with neurodegenerative conditions, including Parkinson's and Alzheimer's diseases. As shown in the figure, differentially expressed genes related to neurological disorders from RNA-seq analysis exhibited consistent up- or downregulation trends with qRT–PCR validation (Fig. 6). This confirmed the accuracy of the RNA-seq data, suggesting that *N. farcinica* infection via the intravenous route might induce neurological impairment and trigger neurodegenerative diseases. We analyzed differentially expressed genes related to neurodegenerative diseases and generated a heatmap (Fig. 7A). The heatmap highlighted the clustering of neurodegenerative disorders, such as Alzheimer's and Parkinson's diseases. Additionally, we conducted protein-protein interaction (PPI) analysis on differentially expressed genes associated with

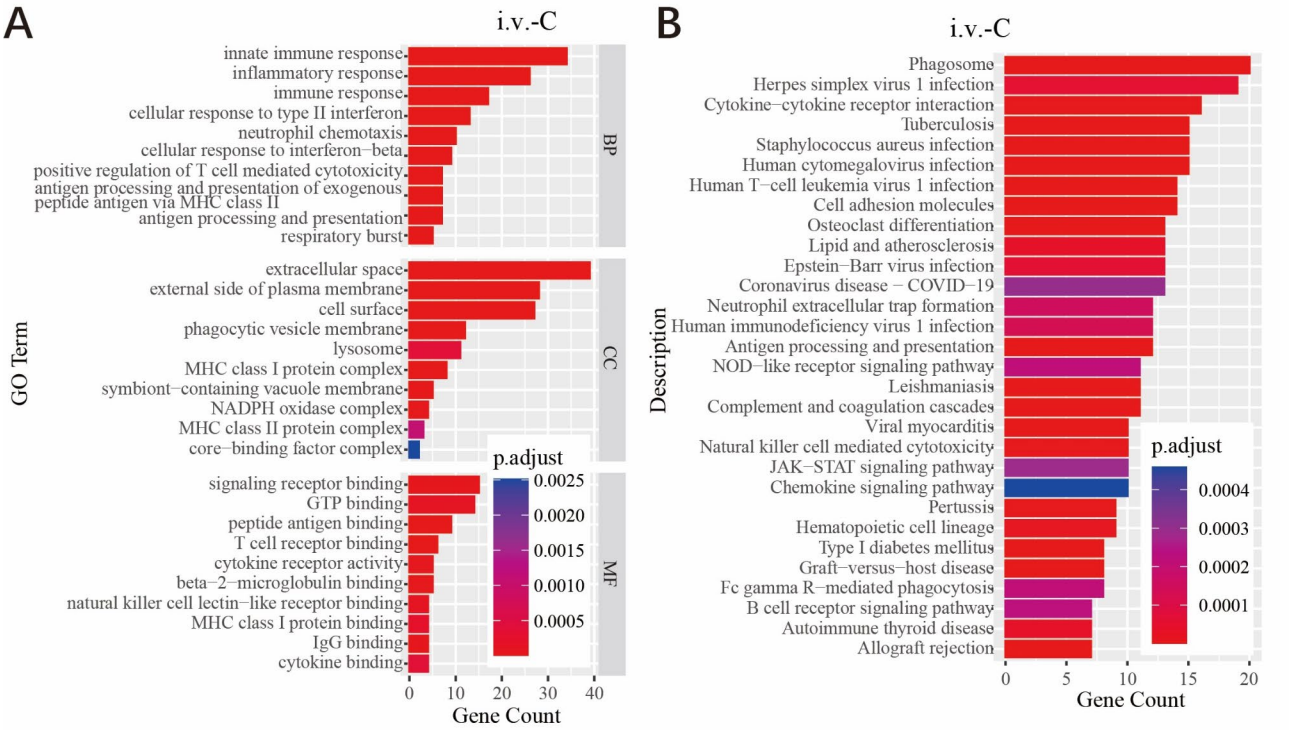

Fig. 5 Transcriptomic analysis of brain tissues infected with *N. farcinica*. (**A**) GO analysis of *N. farcinica* infected via intravenous infection. BP (Biological Process), CC (Cellular Component), MF (Molecular Function). (**B**) DEGs KEGG pathway analysis of *N.farcinica* infected by intravenous infection pathway

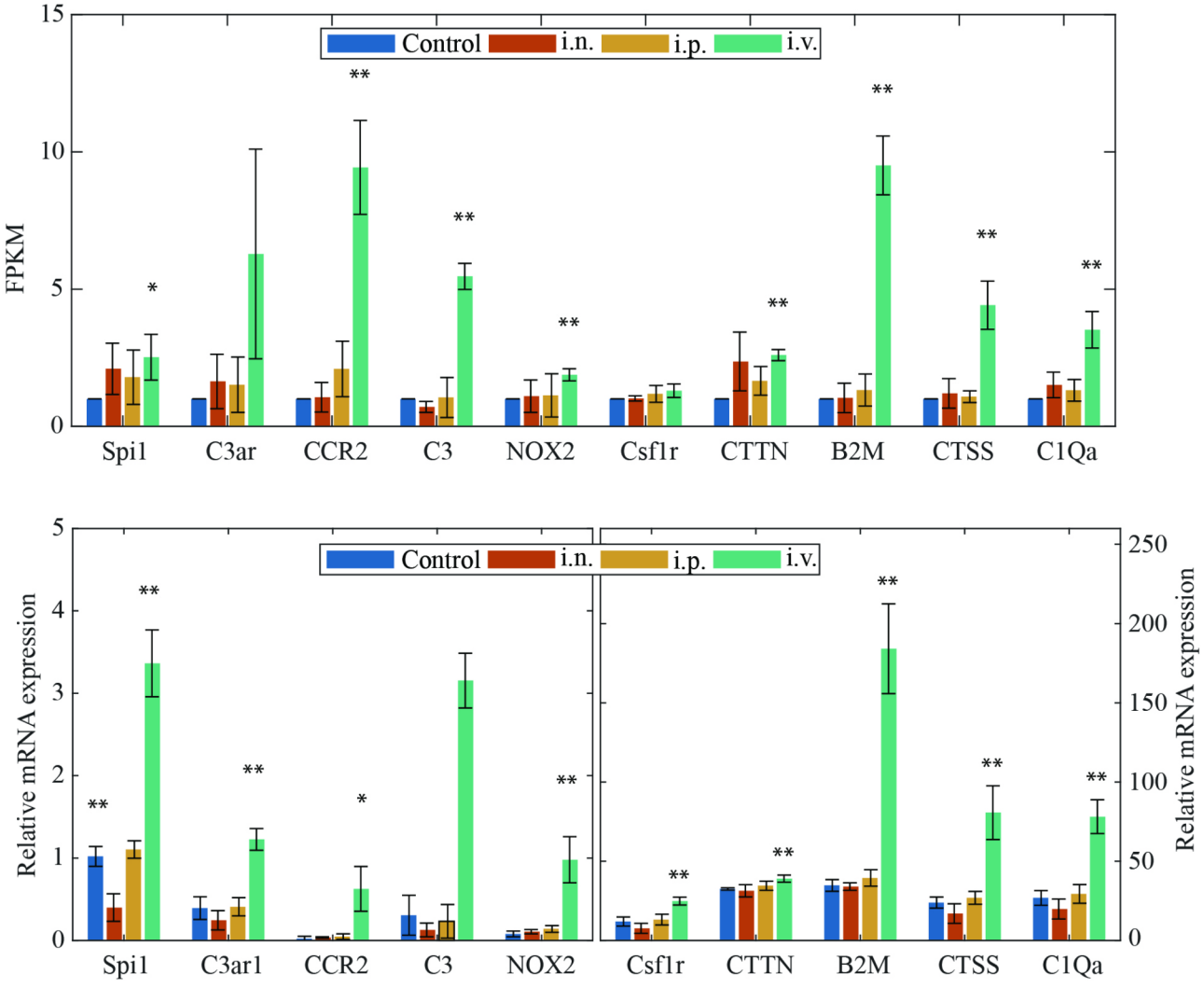

Fig. 6 The genes involved in neurodegenerative diseases were analyzed by RNA-seq and verified by qRT–PCR. $P<0.05$ or 0.01 and marked by * or **, respectively

the nervous system and neurodegenerative diseases during *N. farcinica* infection (Fig. 7B). As shown in Fig. 7B, among the differentially expressed genes associated with neurological disorders and neurodegenerative diseases, IL1B, CSF1R, and SPI1 might play important roles in the progression of *N. farcinica* infection.

Discussion

Animal models that enable reproducible measurements of disease progression and pathology are essential for developing new therapies, vaccines, and diagnostic assays for nocardiosis. Using BALB/c mice, we measured empirical clinical signs of infection, such as weight loss and other metrics, to qualify and quantify pathological differences. Based on preliminary experiments, 1×10^7 CFU *N. farcinica* was selected for intravenous infection. This infection dose resulted in the death of some mice (approximately 2/10), accompanied by pronounced neurological symptoms, consistent with previous research [18]. As a positive control to simulate a similar mortality rate to intravenous infection, a dose of 1×10^8 CFU *N. farcinica* was used for intraperitoneal infection. Additionally, to compare the effects of intranasal infection with an equivalent dose to intravenous infection, 1×10^7 CFU was used for intranasal infection. The results showed that the *N. farcinica* inoculation route had a significant impact on the outcome in mice. Intravenous infection resulted in more pronounced clinical symptoms, inflammatory response, tissue lesions, higher mortality rate, and bacterial load compared to intranasal infection. After intranasal inoculation, mice exhibited increased body temperature and decreased body weight at 1 and 2 dpi. This infection route caused pronounced lung inflammation and significant pathological alterations, with relatively less damage to other organs. Although *N. farcinica* was not detected in the brain,

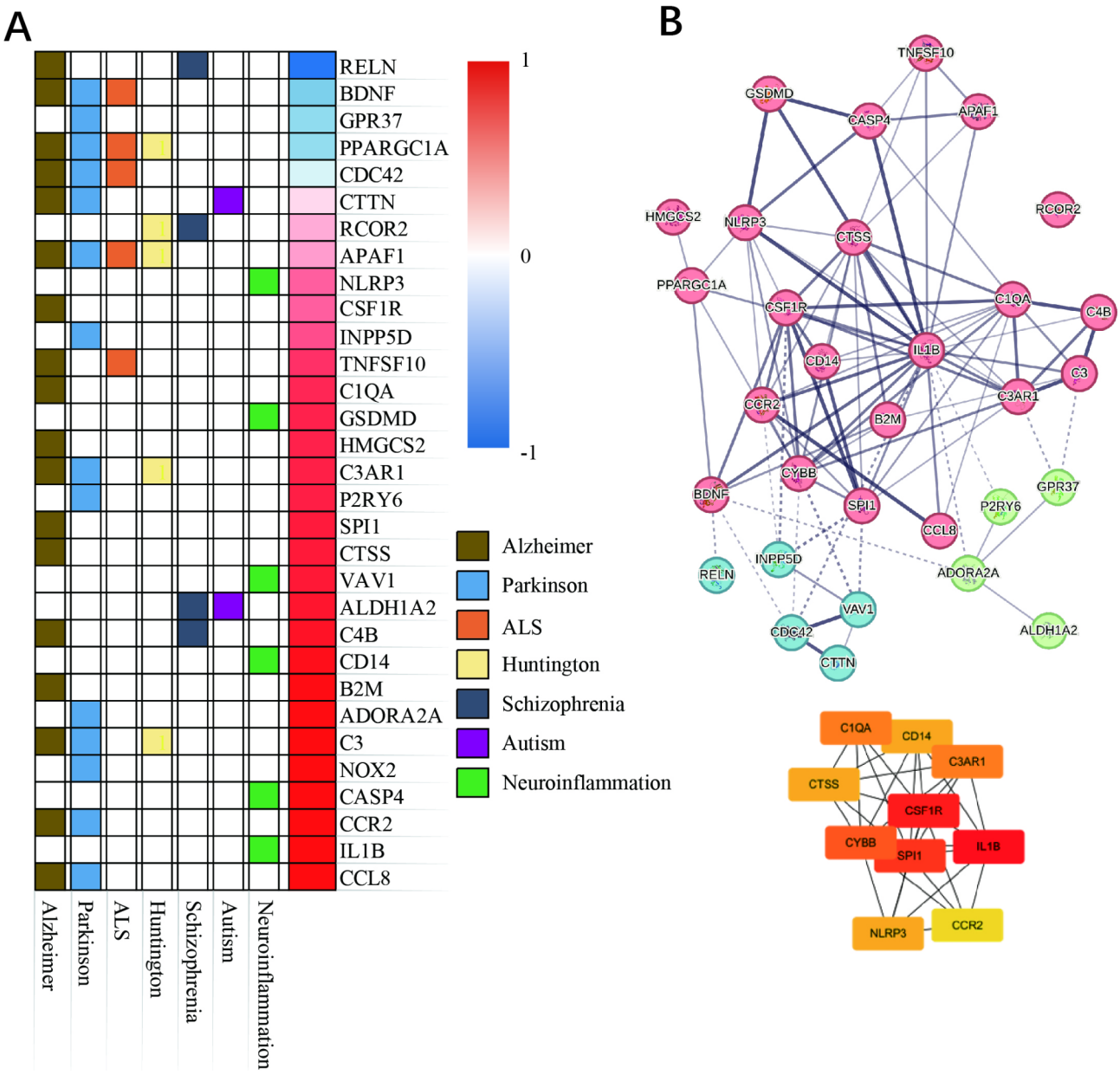

Fig. 7 (**A**) Heatmap of the DEGs related to neurodegenerative diseases. (**B**) Protein-protein interaction network of genes associated with the nervous system and neurodegenerative diseases, along with ten hub genes

minor pathological changes were observed. This discrepancy between histopathology and CFU count suggests that the clinical effect of infection is influenced more by the host immune response than by bacterial load alone [19]. Cytokine changes in serum showed that only IL-4 and IL-6 levels increased. It is speculated that the lower infection dose and lung-restricted infection in immunocompetent mice may hinder the development of disseminated infection and systemic symptoms. Consequently, no significant pathogenicity was observed in other organs [18]. This also suggests that IFN-γ and TNF-α were not significantly upregulated due to the mild inflammatory response.

Intravenous infection caused severe systemic infection with obvious clinical symptoms, including elevated body temperature, weight loss, and significant upregulation of cytokines (IL-4, IL-6, IL-10, TNF-α, IFN-γ). Extensive *Nocardia* spp. biofilm formation was observed on a central venous catheter in a cancer institution [20]. A case of catheter-related bloodstream infection caused by *N. farcinica* was also reported [21]. In this study, intravenous infection with *N. farcinica* invaded all organs,

consistent with previous reports [22]. Some mice experienced elevated body temperature after infection, followed by a sudden drop accompanied by neurological symptoms, leading to death the next day. This suggests that the immune system struggles to combat *N. farcinica* infection, with bacterial replication outpacing the body's clearance mechanisms. Since hypothermia is a significant sign of sepsis, it is speculated that the body progressed to sepsis at this point, leading to a drastic drop in rectal temperature and eventual death [23]. Additionally, it has been reported that intravenous inoculation of *Nocardia asteroides* in experimental animals leads to preferential invasion and proliferation in specific anatomical regions, particularly the brain [24]. In this study, *N. farcinica* invasion exhibited a similar pattern, with more severe neurological symptoms and higher bacterial loads in the brain observed in cases of intravenous infection compared to the other two infection routes. A notable observation was the increased bacterial burden in the kidneys. Histopathological examination of the kidney revealed worsening pathology from 1 to 7 dpi (Supplementary Fig. 1). A similar phenomenon was observed in mice infected with Serratia marcescens via intravenous injection [25]. This may result from the increased replication rate of *N. farcinica* in mice infected via the tail vein or the host's inadequate immune clearance, leading to unchecked bacterial proliferation. The specific mechanisms underlying this phenomenon deserve further investigation. Although the inoculum dose was equivalent between the intranasal and tail vein infection routes, the number of *N. farcinica* that breach tissue and disseminate depends on the immune defense capability at each port of entry.

In this study, we found that the bacterial burden in the rectum was higher in intraperitoneal infection compared to the other two infection routes. Purulent secretion in the anus was observed, leading to defecation difficulty, and severe pathological changes in the tissue. To our knowledge, intestinal damage caused by *Nocardia* infection has not been previously reported. Ocular involvement by *Nocardia* spp. has been documented only in isolated cases and not confirmed by experimental research [26]. We found that *N. farcinica* could spread to the eye and multiply following both intravenous and intraperitoneal infection, manifesting clinical symptoms. Ji et al. reported that *N. farcinica* can quickly cross the blood-brain barrier and enter the brain parenchyma, causing CNS infection through intravenous injection, findings replicated in our study using intraperitoneal infection [18]. Similarly, our study replicated these findings using intraperitoneal infection, although it required a higher bacterial dose.

Transcriptome analysis revealed that only intravenous infection through the tail vein enriched multiple differentially expressed genes. Biological Process (BP) enrichment highlighted significant involvement of innate and adaptive immune responses, consistent with research on the brain's complex immune regulatory mechanisms [27]. Cellular Component (CC) enrichment points to specific subcellular compartments and organelles involved in immune responses, while Molecular Function (MF) enrichment emphasizes the dynamic molecular interactions underlying immune regulation in the brain, consistent with immune cell activation [28, 29]. Furthermore, terms such as "cellular response to type II interferon" and "neutrophil chemotaxis" suggest the activation of immune signaling pathways and cell recruitment, consistent with their roles in neuroinflammation [30, 31].

KEGG pathway enrichment analysis highlighted the involvement of multiple immune response pathways, emphasizing the central role of immune cell communication and activation in response to *N. farcinica* infection [32]. Pathways such as "Tuberculosis," "Graft−versus−host disease," and "Type I diabetes mellitus" suggest a possible link between *N. farcinica*-induced neuroinflammation and broader systemic immune responses [33, 34]. Pathways such as the "NOD−like receptor signaling pathway" and "Antigen processing and presentation" imply the activation of innate immune mechanisms and antigen recognition within the brain [35]. Interestingly, the enrichment of pathways related to neutrophil functions may indicate the involvement of neutrophils in *N. farcinica*-induced neuroinflammatory processes [36]. These findings illustrate the complexity of the brain's immune microenvironment and its potential impact on neurological and systemic health following intravenous *N. farcinica* infection.

Among the 187 DEGs identified from transcriptomic analysis, 31 genes associated with neurological disorders were selected for constructing heatmaps and protein-protein interaction networks. PPI analysis and heatmap visualization suggest that *N. farcinica* infection in mice can induce neurodegenerative disorders. Their central positions within the PPI network highlight their potential significance as key regulators in the complex interplay of factors driving *N. farcinica*-induced neurological diseases. The involvement of these genes in neurodegenerative disorders has also been documented [37–39]. Elucidating the in-depth pathogenic mechanisms will be the focus of our future research.

Conclusion

This study highlights the significant impact of infection routes on the pathogenicity of *N. farcinica* in BALB/c mice. Of the tested routes, intravenous infection was the most severe, as reflected in the extent of infection, tissue colonization, and inflammation within the host. This study provides a theoretical foundation for understanding the pathogenicity of *N. farcinica* across different

infection routes and offers critical insights for developing targeted clinical interventions and improving nocardiosis management.

Supplementary Information

The online version contains supplementary material available at https://doi.org/10.1186/s12879-024-09877-x.

Supplementary Material 1

Supplementary Material 2

Author contributions

Study concept and design: J. S., L. H., and Z. L. Acquisition of data: J. S., L. H., and Y. J. Analysis and interpretation of data: J. S. and S. X. Drafting of the manuscript: J. S., X. L., and F. L. Critical revision of the manuscript for important intellectual content: X. Q. and Z. L.

Funding

This work is supported by National Natural Science Foundation of China (L2124006) and the National Key Research and Development Plan of China (NO.2021YFC2301001).

Data availability

Data is provided within the manuscript or supplementary information files.

Declarations

Consent for publication

Not applicable.

Ethical approval

Animal experiments conducted in this study were approved by the Ethics Review Committee of the National Institute for Communicable Disease Control and Prevention in the Chinese Center for Disease Control and Prevention, with approval number 2022-042. The study was conducted in compliance with the ARRIVE guidelines and the National Institutes of Health guide for the care and use of Laboratory animals.

Competing interests

The authors declare no competing interests.

Received: 24 December 2023 / Accepted: 4 September 2024
Published online: 20 September 2024

References

1. Roussel X, Daguindau E, Berceanu A, Desbrosses Y, Saas P, Ferrand C, et al. Altered thymic CD4 + T-cell recovery after allogeneic hematopoietic stem cell transplantation is critical for nocardiosis. Curr Res Transl Med. 2019;67:135–43.
2. Hashemzadeh M, Dezfuli AAZ, Khosravi AD, Savari M, Jahangirimehr F. Genotypic and phenotypic prevalence of *Nocardia* species in Iran: first systematic review and meta-analysis of data accumulated over years 1992–2021. PLoS ONE. 2021;16:e0254840.
3. Nakamura I, Nagakura T, Fujita H, Fukusima S, Gonoi T. *Nocardia* elegans infection: a case report and literature review. Int J Infect Dis. 2017;54:15–7.
4. Inamadar AC, Palit A. Primary cutaneous nocardiosis: a case study and review. Indian J Dermatol Venereol Leprol. 2003;69:386–91.
5. Huang L, Chen X, Xu H, Sun L, Li C, Guo W, et al. Clinical features, identification, antimicrobial resistance patterns of *Nocardia* species in China: 2009–2017. Diagn Microbiol Infect Dis. 2019;94:165–72.
6. Peleg AV, Husain S, Qureshi ZA, Silveira FP, Sarumi M, Shutt KA, et al. Risk factors, clinical characteristics, and outcome of *Nocardia* infection in organ transplant recipients: a matched case-control study. Clin Infect Dis. 2007;44:1307–14.
7. Restrepo A, Clark NM. *Nocardia* infections in solid organ transplantation: guidelines from the infectious diseases Community of Practice of the American Society of Transplantation. Clin Transpl. 2019;33:e13509.
8. Williams E, Jenney AW, Spelman DW. *Nocardia* bacteremia: a single-center retrospective review and a systematic review of the literature. Int J Infect Dis. 2020;92:197–207.
9. Spoleti MJ, Vidal ME, Ruiz F. Intra-abdominal infections in pediatrics. Int J Infect Dis. 2018;73:328–9.
10. Li SY, Yu KW, Yang WC, Chen TW, Lin CC. *Nocardia* peritonitis - a case report and literature review. Perit Dial Int. 2008;28:544–7.
11. Corti ME, Villafañe Fioti MF. Nocardiosis: a review. Int J Infect Dis. 2003;7:243–50.
12. Bromage ES, Owens L. Infection of barramundi lates calcarifer with Streptococcus iniae: effects of different routes of exposure. Dis Aquat Organ. 2002;52:199–205.
13. Nair N, Guedes MS, Werts C, Gomes-Solecki M. The route of infection with leptospira interrogans serovar copenhageni affects the kinetics of bacterial dissemination and kidney colonization. PLoS Negl Trop Dis. 2020;14:1–13.
14. Nelson M, Burton N, Nunez A, Butcher W, Ngugi S, Atkins TP. Efficacy of co-trimoxazole against experimental melioidosis acquired by different routes of infection. Antimicrob Agents Chemother. 2022;66:e00708–22.
15. Joshua S, Babu R, Warrier A, Panikar D. *Nocardia* araoensis causing brain abscess. Asian J Neurosurg. 2019;14:952–6.
16. Ogata SA, Beaman BL. Adherence of *Nocardia asteroides* within the murine brain. Infect Immun. 1992;60:1800–5.
17. Kohbata S, Beaman BL. L-Dopa-responsive movement disorder caused by *Nocardia asteroides* localized in the brains of mice. Infect Immun. 1991;59:181–91.
18. Ji X, Han L, Zhang W, Sun L, Xu S, Qiu X, et al. Molecular, cellular and neurological consequences of infection by the neglected human pathogen *Nocardia*. BMC Biol. 2022;20:1–17.
19. Dormans J, Burger M, Aguilar D, Hernandez-Pando R, Kremer K, Roholl P, et al. Correlation of virulence, lung pathology, bacterial load and delayed type hypersensitivity responses after infection with different *Mycobacterium tuberculosis* genotypes in a BALB/c mouse model. Clin Exp Immunol. 2004;137:460–8.
20. Wenger PN. Nocardia farcinica sternotomy site infections in patients following open heart surgery. J Infect Dis. 1998;178:1539–43.
21. Heo ST, Ko KS, Kwon KT, Ryu SY, Bae IG, Oh WS, et al. The first case of catheter-related bloodstream infection caused by *Nocardia farcinica*. J Korean Med Sci. 2010;25:1665–8.
22. Torres OH, Domingo P, Pericas R, Boiron P, Montiel JA, Vázquez G. Infection caused by *Nocardia farcinica*: Case report and review. Eur J Clin Microbiol Infect Dis. 2000;19:205–12.
23. Tian H, Zhang M, Du C, Li D, Zhou Q, Wu L, et al. Effects of rhubarb combined with ulinastatin on T-cell subsets in sepsis rats. Int J Clin Exp Med. 2015;8:1234–40.
24. Beaman BL, Boiron P, Beaman L, Brownell GH, Schaal K, Gombert ME. *Nocardia* and nocardiosis. Med Mycol. 1992;30:317–31.
25. Anderson MT, Brown AN, Pirani A, Smith SN, Photenhauer AL, Sun Y, et al. Replication dynamics for six gram-negative bacterial species during bloodstream infection. MBio. 2021;12:e01114–21.
26. Garg P. Fungal, *mycobacterial*, and *Nocardia* infections and the eye: an update. Eye. 2012;26:245–51.
27. Weiss F, Labrador-Garrido A, Dzamko N, Halliday G. Immune responses in the Parkinson's disease brain. Neurobiol Dis. 2022;168:e105700.
28. Woodard GE, Jardín I, Berna-Erro A, Salido GM, Rosado JA. Regulators of G-Protein-signaling proteins: negative modulators of G-Protein-coupled receptor signaling. Int Rev Cell Mol Biol. 2015;317:97–183.
29. Mino T, Takeuchi O. Post-transcriptional regulation of immune responses by RNA binding proteins. Proc Japan Acad Ser B Phys Biol Sci. 2018;94:248–58.
30. Hume DA, Schroder K, Hertzog PJ, Ravasi T. Interferon-gamma: an overview of signals, mechanisms and functions. J Leukoc Biol. 2004;75:163–89.
31. Stephenson J, Nutma E, van der Valk P, Amor S. Inflammation in CNS neurodegenerative diseases. Immunology. 2018;154:204–19.
32. Li WC, Bai DL, Xu Y, Chen H, Ma R, Hou WB, et al. Identification of differentially expressed genes in synovial tissue of rheumatoid arthritis and osteoarthritis in patients. J Cell Biochem. 2019;120:4533–44.
33. Mayer-Barber KD, Barber DL. Innate and adaptive Cellular Immune responses to *Mycobacterium tuberculosis* infection. Cold Spring Harb Perspect Med. 2015;5:a018424.

34. Bluestone JA, Buckner JH, Herold KC, Immunotherapy. Building a bridge to a cure for type 1 diabetes. Sci (80-). 2021;373:510–6.
35. Wagner CS, Cresswell P. TLR and nucleotide-binding oligomerization domain-like receptor signals differentially regulate exogenous Antigen Presentation. J Immunol. 2012;188:686–93.
36. Chou M-L, Babamale AO, Walker TL, Cognasse F, Blum D, Burnouf T. Blood–brain crosstalk: the roles of neutrophils, platelets, and neutrophil extracellular traps in neuropathologies. Trends Neurosci. 2023;46:764–79.
37. Corces MR, Shcherbina A, Kundu S, Gloudemans MJ, Frésard L, Granja JM, et al. Single-cell epigenomic analyses implicate candidate causal variants at inherited risk loci for Alzheimer's and Parkinson's diseases. Nat Genet. 2020;52:1158–68.
38. Spangenberg E, Severson PL, Hohsfield LA, Crapser J, Zhang J, Burton EA, et al. Sustained microglial depletion with CSF1R inhibitor impairs parenchymal plaque development in an Alzheimer's disease model. Nat Commun. 2019;10:e3758.
39. Mackenzie IRA. Anti-inflammatory drugs and Alzheimer-type pathology in aging. Neurology. 2000;54:732–4.

Publisher's note

Springer Nature remains neutral with regard to jurisdictional claims in published maps and institutional affiliations.